Materials Innovations

HΣXA Publishers

Dielectric Materials | Research Article | http://doi.org/10.54738/MI.2022.2201

Barium Doping Effects on Frequency-dependent Dielectric Properties of Cobalt Ferrite Nanoparticles

Mubasher[1]*, Muhammad Mumtaz[1]*, Arslan Bashir[1], Muhammad Rashid[1], Tayyab Umar[1], Zahid Sarfraz[2], Hamid Zia[1]

1 Department of Physics, Faculty of Basic and Applied Sciences (FBAS), International Islamic University (IIU), H10, 44000, Islamabad, Pakistan
2 Department of Physics, Air University, E9, 44000, Islamabad, Pakistan

Received: 01 February 2022
Accepted: 21 February 2022
Published: 28 February 2022

Citation: Mubasher , Mumtaz M, Bashir A, Rashid M, Umar T, Sarfraz Z, Zia H (**2022**) Barium Doping Effects on Frequency-dependent Dielectric Properties of Cobalt Ferrite Nanoparticles. *Materials Innovations 2* (3), 1-10.

***Correspondences**: (Mubasher) mubi862008@gmail.com (Muhammad Mumtaz) mmumtaz75@yahoo.com

Published By Hexa Publishers

ISSN
Electronic: 2790-1963

The chemical solgel method was employed for the preparation of barium doped cobalt ferrite ($Co_{1-x}Ba_xFe_2O_4$) nanoparticles. Different concentrations of barium were doped in cobalt ferrites "$CoFe_2O_4$" nanoparticles to get $Co_{1-x}Ba_xFe_2O_4$; x = 0, 0.25, 0.50, 0.75 and 1.0 nanoparticles. X-ray diffraction (XRD) spectroscopy was employed for the analysis of crystallographic structure and Debye-Scherrer formula was employed for the determination of average crystallite size. The morphological study and size calculation of $Co_{1-x}Ba_xFe_2O_4$ nanoparticles were carried out by using scanning electron microscopy (SEM). Energy dispersive X-ray (EDX) spectroscopy was used for the compositional analysis of these nanoparticles. The vibrational modes of different atoms present in these nanoparticles were investigated using Fourier transform infrared (FTIR) spectroscopy. The dielectric parameters such as capacitance, real and imaginary parts of dielectric constant, loss tangent and ac-conductivity were inspected using LCR meter. Significant improvement in charge storage and transport properties were achieved with the doping of barium in $CoFe_2O_4$ nanoparticles.

Keywords: Transport properties, Dielectric parameters, Polarization, Cobalt ferrite nanoparticles, Barium doped cobalt ferrite nanoparticles

INTRODUCTION

Ferrites having ferromagnetic or ferrimagnetic nature are the significant class of nanomaterials that exhibit a variety of characteristics and displayed exciting scientific and industrial applications. The ferrimagnetic materials confined to nanoscale are considered as promising choice owed to their diverse applications that spanned from magnetic devices like non-volatile magnetic storage media to high-frequency devices.[1–4] The prominent features that distinguish ferrites from other metallic counterparts are lower eddy-current loss, high electrical resistivity, strong dielectric properties, a strong coercive field, high-frequency permeability and high chemical stability.[5–8] Due to these features, ferrites are widely researched in electrochemical science and technology,

solid-state electronics, magnetics, magneto-electronics and biotechnology. The structural and chemical modifications, such as insertion, doping and hybridization of ferrites have led to their increased demands due to highly tuned physical and chemical properties.[9–18] Furthermore, the substitution of other divalent or trivalent metals with variable electronegativities and ionic-radii in ferrites gave appreciating results in tuning and improving their properties.[21–23] In ferrites, $CoFe_2O_4$ nanoparticles are considered a viable contender in the field of memory as well as energy storage devices due to their high cubic magneto-crystalline anisotropy and excellent chemical stability. In $CoFe_2O_4$ nanoparticles, Co^{2+} ions occupy octahedral B-sites in the spinel structure, whereas Fe^{2+} ions are distributed evenly between tetrahedral A-sites and octahedral B-sites just like many other ferrites.[19,20] The Gd doped $CoFe_2O_4$ nanoparticles were synthesized to investigate the structural, electrical conduction and dielectric properties using solid-state reaction method. The dielectric analysis of pure $CoFe_2O_4$ nanoparticles indicated that pure $CoFe_2O_4$ nanoparticles have two dielectric relaxations in 1–10 kHz frequency range, while Gd doped $CoFe_2O_4$ nanoparticles have single relaxation at 1 kHz. The dielectric constant of $CoFe_{2-x}Gd_xO_4$ ceramics was higher than that of pure $CoFe_2O_4$ nanoparticles which attributed to lattice distortion caused by Gd inclusion.[24] The structural, dielectric and magnetic properties of Pr / Yb doped $CoFe_2O_4$ and $PbZrTiO_3$ nanoparticles were investigated. The morphological investigations revealed homogeneous distribution of parent phase grains in these composites. The dielectric measurements indicated diffused phase shift at a specified frequency (100 kHz) which direct ferroelectric to paraelectric phase transition.[25] The structural and electrical properties of nickel and zinc doped $CoFe_2O_4$ nanoparticles were investigated. The existence of interfacial and dipolar polarization in the prepared nanoparticles ascribed higher values of dielectric permittivity at lower frequency regime. The calculations of activation energy indicated that similar nature of charge carriers accounted for the relaxation as well as conduction processes.[26] The influence of Yttrium substitution on the crystal structure, optical as well as relaxation behavior of $CoFe_2O_4$ nanoparticles were investigated using citrate auto-ignition synthesis route. The study was conducted to find the non-debye relaxation behavior through in-depth relaxation mechanism. The Havriliak-Negami formalism was employed to describe the relaxation mechanism in the dielectric analysis.[27] The incorporation of rare-earth ions with spinel ferrites enhanced the dielectric parameters, resistivity and decreased dielectric losses, depending on the ionic size and concentration of inserted element. Additionally, the differences in ionic size of dopants and doped materials can cause lattice distortions that have significant impact on charge storage properties.[28] Thus, it can be concluded that the doping of different ferrites with various other ferrites, ions or metal is a well-recognized and adaptable method of tuning the structure and physical properties.[22–28] The current research work is focused to investigate the influence of barium (Ba) doping on the structural, morphological as well as dielectric properties of $CoFe_2O_4$ nanoparticles. The key objective of this work is to analyze the dielectric properties of $CoFe_2O_4$ nanoparticles that can be tuned with the doping of barium. The barium doping in $CoFe_2O_4$ nanoparticles is predicted to produce structural disorder and lattice strain that can have significant impact on electrical conduction of $Co_{1-x}Ba_xFe_2O_4$; x = 0, 0.25, 0.50, 0.75 and 1.0 nanoparticles.

EXPERIMENTAL SETUP

The chemical solgel technique was employed for the synthesis of $Co_{1-x}Ba_xFe_2O_4$; x = 0, 0.25, 0.50, 0.75 and 1.0 nanoparticles. The synthesis of these nanoparticles was started by taking two beakers (A and B). The 20mL ethanol was taken in beaker A and placed on hot plate magnetic stirrer with calculated amount of cobalt nitrate [Co $(NO_3)_2.6H_2O$], barium nitrate [Ba $(NO_3)_2$]and iron nitrate [Fe $(NO_3)_3$] in beaker A for 30 minutes. The 20mL distilled water was taken in beaker B alongwith the calculated amount of citric acid ($C_6H_8O_7$) having molar mass 192.12 g/mol for 20 minutes. Afterwards, pour attained homogeneous solutions of beaker B into beaker A drop by drop. Ammonia "NH_3" was added in this solution dropwise until the achievement of pH 7. Then the solution was heated inbetween 80 to 90^{o}C with continuously stirring until gel formation, and then place this gel in microwave oven at 100^{o}C for overnight drying. Later-on, ground the powder using mortar and pestle, and subsequently annealed at 650^{o}C for 4 hours in the tube furnace. Again ground the powder to obtain ultrafine $Co_{1-x}Ba_xFe_2O_4$; x = 0, 0.25, 0.50, 0.75 and 1.0 nanoparticles. The phase confirmation, purity as well as crystal structure of $Co_{1-x}Ba_xFe_2O_4$ nanoparticles were confirmed using XRD technique (Model D/Max IIIC Rigaku) with a CuKα source (wavelength 1.54056 Å). The SEM (Model TESCANVEGA 3) with LaB6 filaments was used for morphological and chemical EDX analysis. The existence of metal-oxygen vibrations was determined using FTIR investigation with a Perklin Elmer spectrum FTIR spectrometer within range of 400 cm^{-1} to 4000 cm^{-1}. LCR meter (Model Hewlett-Packard 4294A) was used for dielectric measurements in the frequency range 1000 Hz to 2 x 10^6Hz.

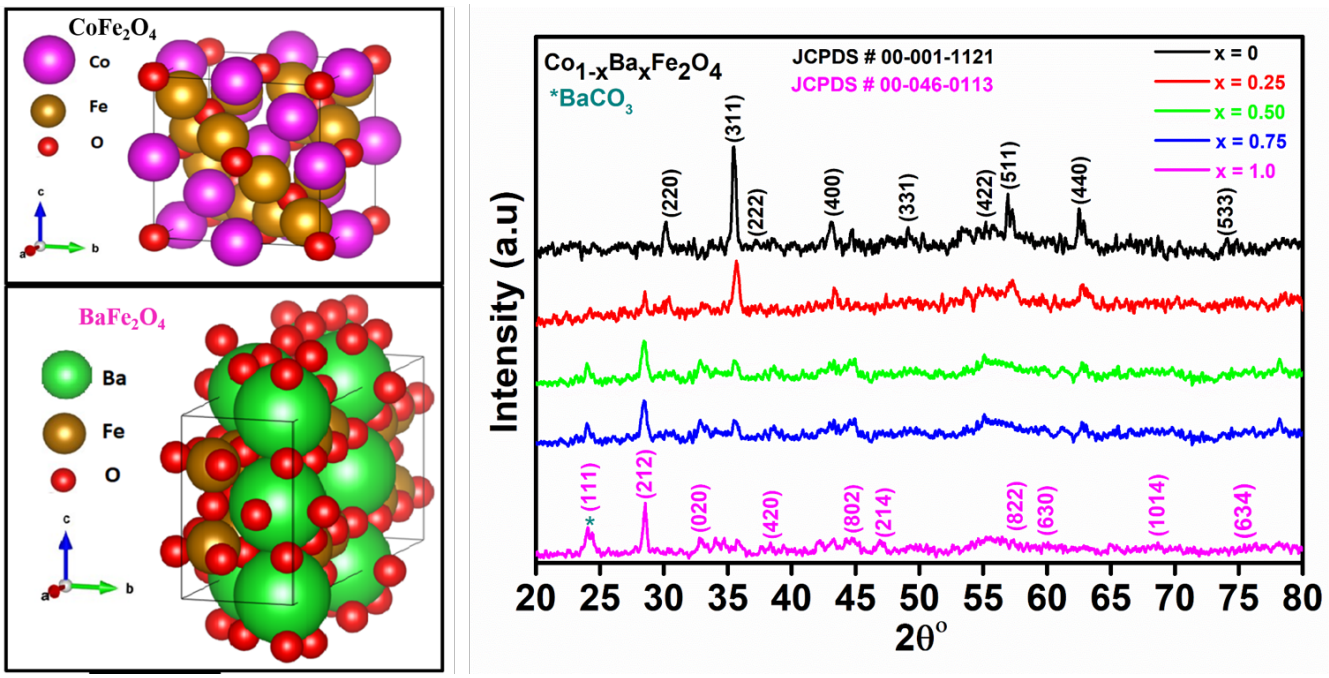

Figure 1. (a) XRD patterns of $Co_{1-x}Ba_xFe_2O_4$; x = 0, 0.25, 0.50, 0.75 and 1.0 nanoparticles, and (b) 3-dimensional structural imagining of pure $CoFe_2O_4$, and $BaFe_2O_4$ nanoparticles.

RESULTS AND DISCUSSION

X-ray diffraction (XRD) is a technique that can be used to study the crystal structure and phase of a material. XRD patterns of $Co_{1-x}Ba_xFe_2O_4$; x = 0, 0.25, 0.50, 0.75 and 1.0 nanoparticles are shown in Figure 1(a). For pure $CoFe_2O_4$ nanoparticles, the peaks at 30.1^o, 35.5^o, 37.3^o, 43.1^o, 49.2^o, 55.1^o, 56.8^o, 62.3^o and 73.9^o correspond to (220), (311), (222), (400), (311), (422), (511), (440) and (533) planes, respectively. These peaks confirmed that $CoFe_2O_4$ nanoparticles have cubic spinel structure in accordance to JCPDS card # 00-001-1121[29,30]. The characteristic peak of $CoFe_2O_4$ nanoparticles was observed at 35.5^o in the diffraction plane (311) as shown in Figure 1(a). For pure barium ferrite ($BaFe_2O_4$) nanoparticles, the obtained peaks were at 28.4^o, 32.7^o, 38.4^o, 44.3^o, 46.9^o, 56.5^o, 59.9^o, 68.7^o and 75.5^o correspond to planes (212), (020), (420), (802), (214), (822), (630), (1014) and (634), respectively. These peaks exactly matched with JCPDS card # 00-046-0113, and the characteristic peak of $BaFe_2O_4$ nanoparticles was at 28.4^o(212)[30]. An extra peak was observed at 24.2^o(111) in XRD spectra of $BaFe_2O_4$ nanoparticles that correspond to $BaCO_3$ [30]. Additionally, the 3-dimensional structures for pure $CoFe_2O_4$ and $BaFe_2O_4$ nanoparticles were visualized from VESTA software and are displayed in Figure 1(b). For $CoFe_2O_4$ nanoparticles, the magnitudes of lattice parameters were found to be a = 8.39 Å, b = 8.39 Å, c = 8.39 Å, and volume of cell was 590.59 x 10^6 (pm^3). On the other hand, lattice parameters magnitudes were established to be a = 19.05 Å, b = 5.39 Å, c = 8.448 Å, and volume of cell was 867.44 x 10^6 (pm^3) for $BaFe_2O_4$ nanoparticles. It is evident from the values of lattice parameters and volume of cell that $CoFe_2O_4$ nanoparticles correspond to cubic structure while $BaFe_2O_4$ nanoparticles exhibited rhombohedral structure, as displayed in Figure 1(b). Furthermore, the crystallite size of $Co_{1-x}Ba_xFe_2O_4$; x = 0, 0.25, 0.50, 0.75 and 1.0 nanoparticles was calculated using Debye-Scherrer formula $\{D=0.9\lambda/\beta\cos\theta\}$[29]. It was observed that with the substitution of barium in $CoFe_2O_4$ nanoparticles, the crystallite size of $Co_{1-x}Ba_xFe_2O_4$ nanoparticles was increased. The increase in crystallite size of $Co_{1-x}Ba_xFe_2O_4$ nanoparticles may be due to the larger atomic radius of barium than $CoFe_2O_4$ nanoparticles.

Scanning electron microscopy (SEM) was performed to study the morphology, shape and size of $Co_{1-x}Ba_xFe_2O_4$ nanoparticles. The SEM images and corresponding histograms of $Co_{1-x}Ba_xFe_2O_4$; x = 0, 0.25, 0.50, and 1.0 nanoparticles were drawn from the particle size using Image J software, as shown in Figure 2 (a-d, $a^{/}$-$d^{/}$). The nanoparticles of uniform grain size and homogeneous morphology are evident from SEM images while minor agglomerations were also noticed in these $Co_{1-x}Ba_xFe_2O_4$ nanoparticles. The average grain size was observed to be 34nm, 27nm, 24nm and 20nm with

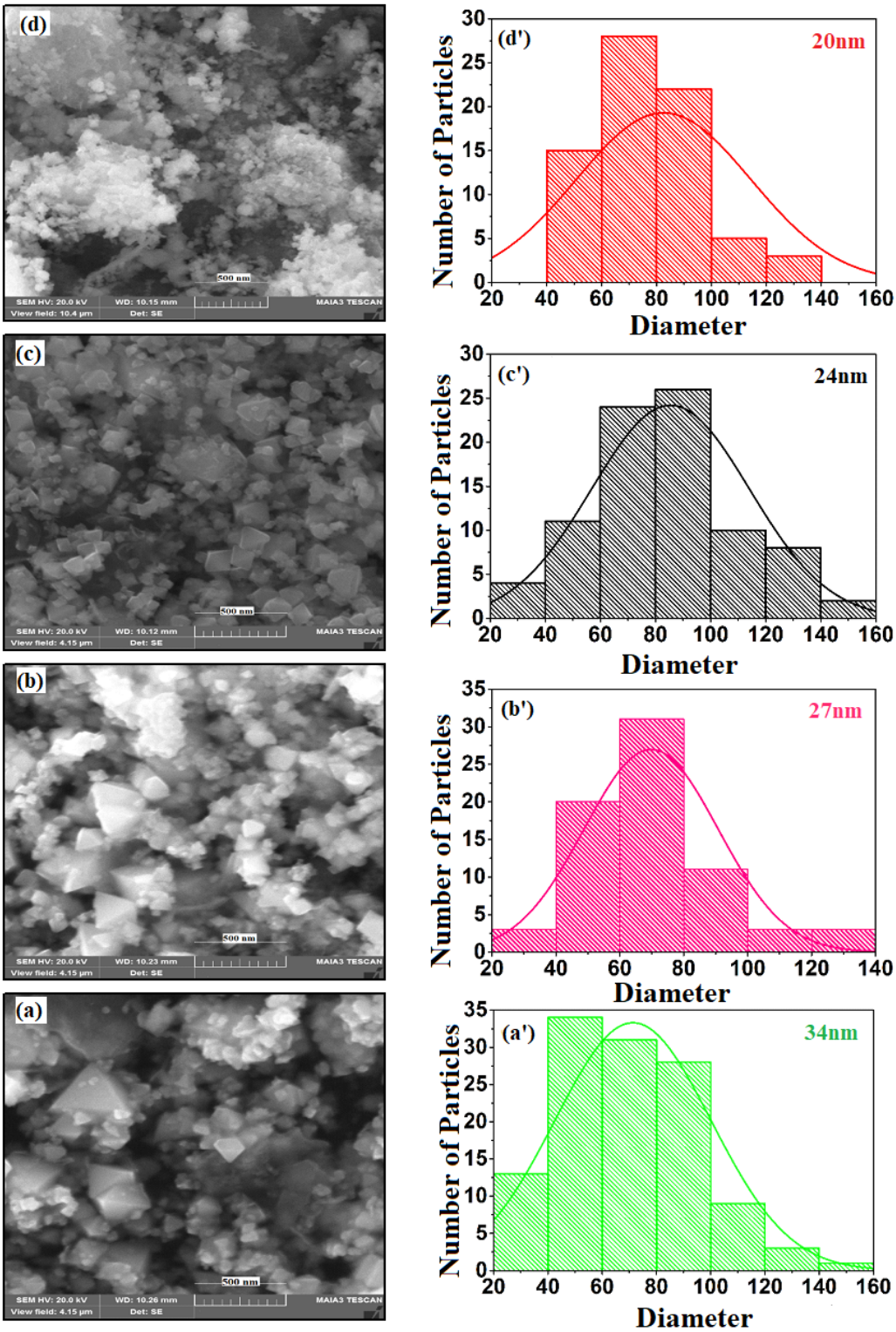

Figure 2. (a-d) SEM images, and (a/-d/) histogramsof $Co_{1-x}Ba_xFe_2O_4$; x = 0, 0.25, 0.50, and 1.0 nanoparticles.

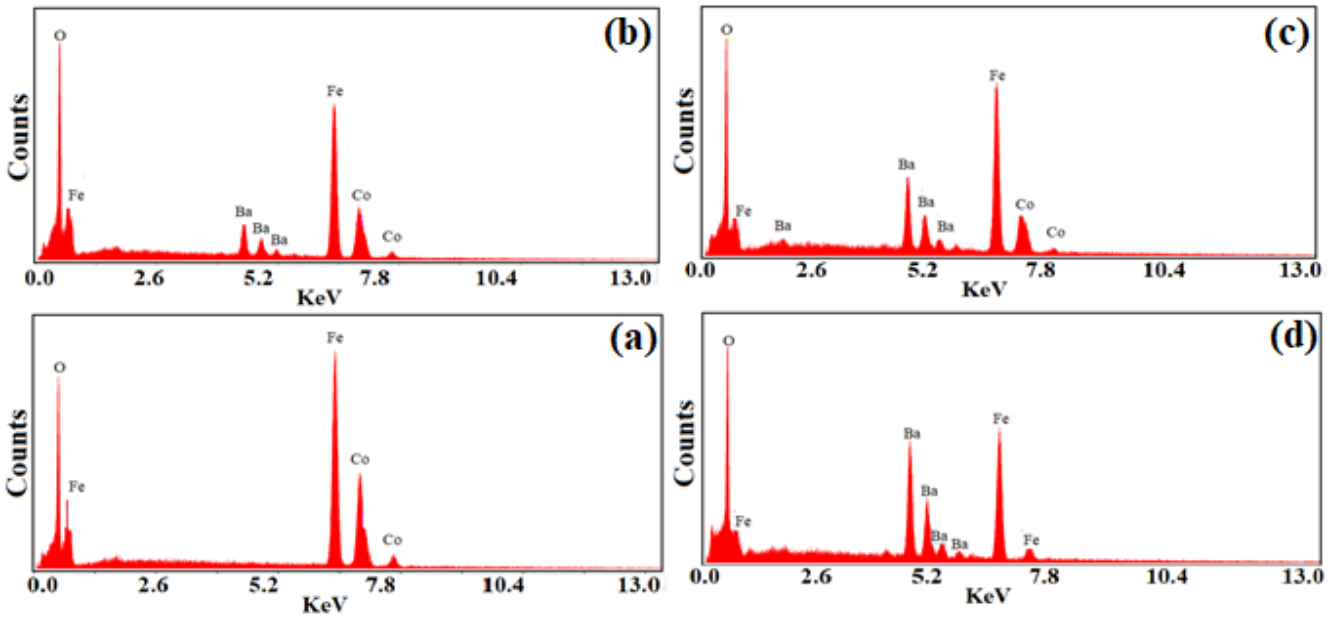

Figure 3. (a-d): EDX spectra of $Co_{1-x}Ba_xFe_2O_4$; x = 0, 0.25, 0.50, and 1.0 nanoparticles.

increasing doping concentrations of barium (x = 0, 0.25, 0.50, and 1.0) in these $Co_{1-x}Ba_xFe_2O_4$ nanoparticles as given in Table 1. Energy dispersive X-rays (EDX) spectroscopy was performed to obtain the elemental composition of $Co_{1-x}Ba_xFe_2O_4$; x = 0, 0.25, 0.50, and 1.0 nanoparticles to identify the presence of any unwanted impurity atoms. The EDX spectra of $Co_{1-x}Ba_xFe_2O_4$; x = 0, 0.25, 0.50, and 1.0 nanoparticles is shown in Figure 3 (a-d). It is evident from Figure 3 (a-d), that only elemental contents of Co, Ba, Fe, and O are present in the EDX spectra of $Co_{1-x}Ba_xFe_2O_4$ nanoparticles. Furthermore, the absence of impurity peaks in the EDX spectra of $Co_{1-x}Ba_xFe_2O_4$ nanoparticles showed that there is no impurity atom present in these nanoparticles which confirmed the high purity of the synthesized nanoparticles.

Fourier transformed infrared (FTIR) spectroscopy is used to reveal the constituent ingredients and nature of a material by inspection of vibrational patterns of atoms. Figure 4 shows the FTIR spectra of the vibrational modes and the chemical bonds of $Co_{1-x}Ba_xFe_2O_4$; x = 0, 0.25, 0.50, 0.75 and 1.0 nanoparticles. The FTIR spectra of ferrites generally show two separate spinel structure bands around 400 cm^{-1} to 600 cm^{-1} which demonstrate the vibrational modes of metal-oxygen bonds at tetrahedral and octahedral lattice sites. The metal oxygen bonds at tetrahedral site generally gave broader band as compared to octahedral site due shorter bond length of the tetrahedral cluster. From the FTIR spectra of $Co_{1-x}Ba_xFe_2O_4$; x = 0, 0.25, 0.50, 0.75 and 1.0 nanoparticles, two broad characteristic bands are identified. The first band appeared in the range between 400 cm^{-1}- 450 cm^{-1} belongs to stretching of metal-oxygen at tetrahedral site, while the second band appeared around 500 cm^{-1} - 550 cm^{-1} corresponds stretching at octahedral site. It is evident from Figure 4 that with increasing concentrations of Barium in $Co_{1-x}Ba_xFe_2O_4$ nanoparticles result in the suppression of these vibrational modes which attributed to the distortions and stresses in the crystal structure originated due to insertion of high ionic radii of Barium in $Co_{1-x}Ba_xFe_2O_4$ nanoparticles.

Capacitance is the ability of the capacitor to store charge when potential difference is applied across its plates. The capacitance of $Co_{1-x}Ba_xFe_2O_4$; x = 0, 0.25, 0.50, 0.75 and 1.0 nanoparticles were measured by using LCR meter. The variation in capacitance (C) with frequency f (Hz) at room temperature is give in Figure 5(a). At low frequency, the values of capacitance are higher and showed depreciation with increasing frequency. This maybe due to the fact that when the frequency increases, the flipping of ac-field become so rapid that the dipoles or charge carriers do not have enough time to flip with applied ac-field due to which polarization decreases, as a result charge-storage capability decreases. This behavior can also be explained with the help of Koops' theory which states that at lower frequencies grains act as conductor, while grain-boundaries as insulator. In low frequency regime, charge carries are piled up at grain-boundaries that enhance the interfacial polarization as a result the storage capacity of the dielectric increases. At higher frequency, the charge carriers could not

Table 1. The variation of grain size, and maximumvalues of C, ε_r', ε_r'', $\tan\delta$ and σ_{ac} of $Co_{1-x}Ba_xFe_2O_4$; x = 0, 0.25, 0.50, 0.75, and 1.0 nanoparticles.

$Co_{1-x}Ba_xFe_2O_4$ nanoparticles	Grain size (nm)	C (1KHz) (F)	ε_r' (1KHz)	ε_r'' (1KHz)	$\tan\delta$ (1KHz)	σ_{ac} (2MHz) $(\Omega m)^{-1}$
x = 0	34	5.57x10-12	9.48	5.7	0.61	5.10x10-5
x = 0.25	27	5.77x10-12	9.81	6.8	0.73	5.60x10-5
x = 0.50	24	6.40x10-12	10.9	16.1	1.41	5.81x10-5
x = 0.75		7.98x10-12	13.6	25.3	1.87	7.92x10-5
x = 1.0	20	1.11x10-11	19	38.8	2.09	1.35x10-4

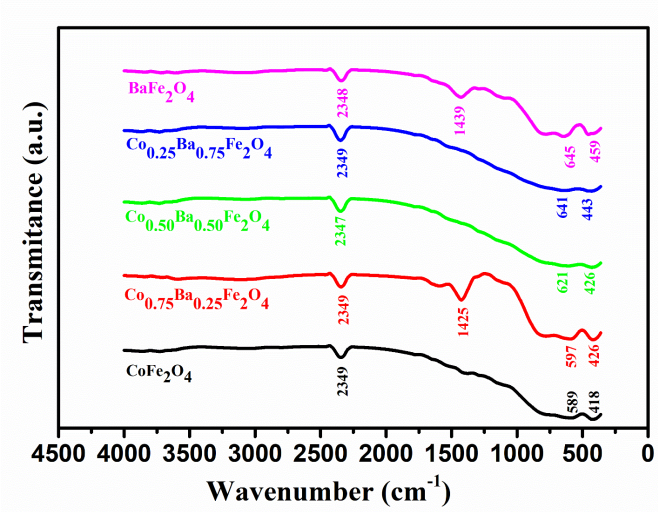

Figure 4. FTIR spectra of $Co_{1-x}Ba_xFe_2O_4$; x = 0, 0.25, 0.50, 0.75 and 1.0 nanoparticles.

reach at the grain boundaries due to lower relaxation time, thus the interfacial polarization could not occur due to which the capacitance of the dielectric decreased. It is evident that $Co_{1-x}Ba_xFe_2O_4$; x = 0.25, 0.50, 0.75 and 1.0 nanoparticles have higher values of capacitance as compared to pure $CoFe_2O_4$ nanoparticles as shown in Figure 5(a). The increase in capacitance with increasing concentrations of barium was observed as shown in the inset of Figure 5(a) and Table 1. The increase in values of capacitance reflected the increased accumulation of charges on the grain boundaries with the doping of barium in $CoFe_2O_4$ nanoparticles. This could also be attributed to the decrease in particle size and lattice distortions produced due to Barium atoms[31]. The decrease in particle size enhanced the surface area which galvanized the grain boundaries effects that resulted in improved capacitance of $Co_{1-x}Ba_xFe_2O_4$ nanoparticles.

When a material is exposed to external electric field some amount of energy stored owing to the charge polarization. This stored energy is represented by real part of the dielectric constant (ε_r') which can be calculated by standard formula $\{\varepsilon_r' = Cd/A\varepsilon_\circ\}$[29]. The variation in $\{\varepsilon_r' = Cd/A\varepsilon_\circ\}$ of $Co_{1-x}Ba_xFe_2O_4$; x = 0, 0.25, 0.50, 0.75 and 1.0 nanoparticles with frequency in the range from 1 kHz to 2 MHz is illustrated in Figure 5(b). It is evident from the graph that ε_r' exhibited high values in low frequency regime which decreased gradually with increase in frequency. The decreasing trend of ε_r' with increasing frequency can be explained using Maxwell-Wagner model and Koops' theory. According to these theories, ferrites are made up of small conducting grains and the separation between the grains are termed as grain boundaries, an insulating or poorly conducting region. The grains play active role whereas the grain boundaries are inactive in low frequency region, so the charge carriers move towards the grain boundaries to produce interfacial polarization which lead to higher values of ε_r'. In high frequency regime, charges could not accumulate at grain boundaries, thus due to lower relaxation time at higher frequency, the values of ε_r' decreases. Increasing trend in the values of ε_r' was observed with the substitution of barium in $CoFe_2O_4$ nanoparticles as shown in Table 1 and inset of Figure 6. This may be due to decrease in particle size, as the surface to volume ratio of nanoparticles increases which is the clear indication of enhancement and intensification of interfaces[19]. The higher distribution of interfaces or grain boundaries in the material enhanced the interfacial

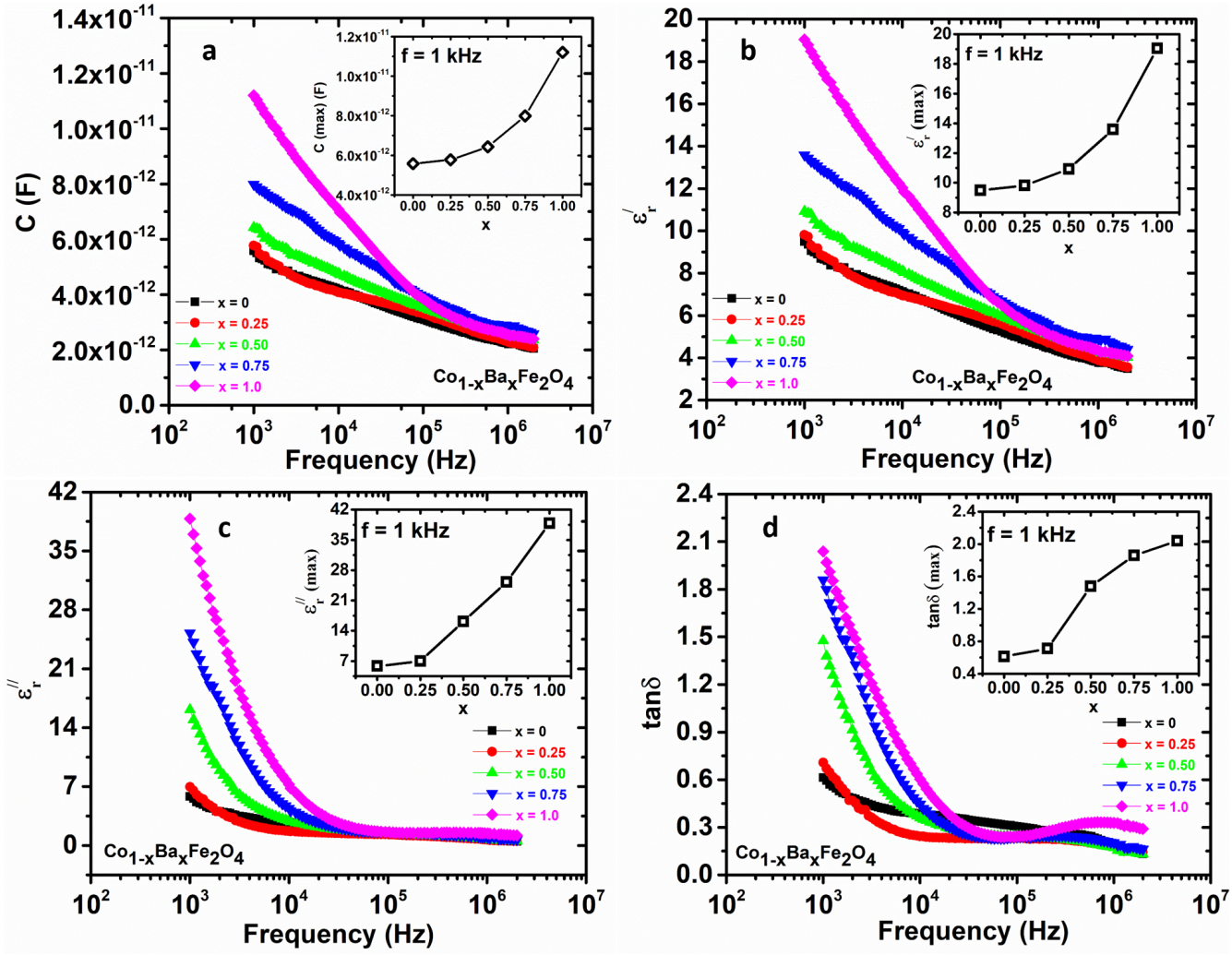

Figure 5. The variation of (a) capacitance (F), (b) $\varepsilon_r^{'}$, (c) $\varepsilon_r^{''}$, (d) $\tan\delta$ verses frequency (Hz) of $Co_{1-x}Ba_xFe_2O_4$; x = 0, 0.25, 0.50, 0.75, and 1.0 nanoparticles.

polarization, as a result, $\varepsilon_r^{'}$ increased with increasing concentration Barium in these $Co_{1-x}Ba_xFe_2O_4$ nanoparticles. When a dielectric material is exposed to an ac-field, apart from charge storage in the form of polarization, some loosely bound charges start to flow in the direction of applied field. Such flow of charges is considered as energy loss and represented by imaginary part ($\varepsilon_r^{''}$) of dielectric constant that can be calculated by standard formula $\{\varepsilon_r^{''} = Gd/A\omega\varepsilon_\circ\}$[29]. The variation in $\varepsilon_r^{''}$ of $Co_{1-x}Ba_xFe_2O_4$; x = 0, 0.25, 0.50, 0.75 and 1.0 nanoparticles with frequency is shown in Figure 5(c). It was observed that the $\varepsilon_r^{''}$ has higher values in low frequency region that deceased with increasing values of frequency, which is well according to Koops' and Wagner models. Furthermore, high energy losses were observed in low frequency region due to higher movement of charge carriers. The interactions of charge carriers with resistive grain boundaries are more frequent in low frequency. The dipoles reorient themselves according to applied ac-field due to which values of $\varepsilon_r^{''}$ are higher in low frequency region. This may also be due to fact that the dipoles oppose each other during flipping, hence, cause loss in energy. At high frequency, charges cannot follow the applied ac-field, thus energy loss decreases due to restricted movement of charges and their interaction with grain boundaries. Table 1 and inset of Figure 5(c) show that pure $CoFe_2O_4$ nanoparticles has lesser value of $\varepsilon_r^{''}$ in $Co_{1-x}Ba_xFe_2O_4$; x = 0.25, 0.50, 0.75 and 1.0 nanoparticles. This may be due to the fact that barium is less electronegative element with high ionic radii than Co, therefore, this could upsurge some loosely bound charge carriers. These charge carriers started to flow and contributed in the energy loss in $Co_{1-x}Ba_xFe_2O_4$ nanoparticles with the provision of external applied ac-field.

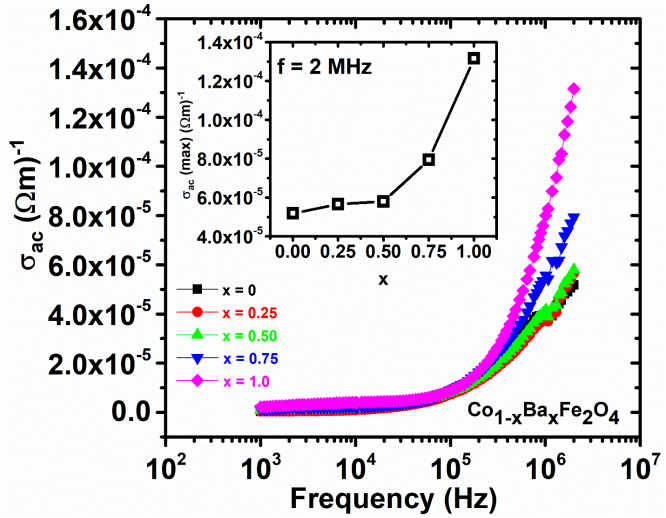

Figure 6. The variation of ac-conductivity(Ωm)$^{-1}$ verses frequency (Hz) of $Co_{1-x}Ba_xFe_2O_4$; x = 0, 0.25, 0.50, 0.75, and 1.0 nanoparticles.

Tangent loss (tanδ) is the energy dissipation arise in any dielectric material with external applied ac-field. The tanδ can be calculated from ratio of imaginary part to the real part of dielectric constant; i.e. $\{\tan\delta = \varepsilon_r''/\varepsilon_r'\}$[29]. The variation in tanδ of $Co_{1-x}Ba_xFe_2O_4$; x = 0, 0.25, 0.50, 0.75 and 1.0 nanoparticles with frequency is shown in Figure 5(d). In low frequency regime, the tanδ exhibited higher values that decreased with higher values of frequency. In low frequency region, the charge carriers and the dipoles follow the external applied ac-field and started to align themselves according to applied field. During the frequent changes in the direction of applied ac-field, the charge carriers and the dipoles also have to change their directions accordingly. Therefore, this process dissipates large amount of energy that can contribute in large tanδ in the low frequency region. The values of tanδ decreases in the high frequency regime as the applied ac-field do not superimpose with frequency of charge carriers or dipoles. The variation in tanδ may also be due to the fact that the heat dissipation and other losses were observed to be lesser because polarization phenomenon decreased owed to the failure of dipoles to track down the rapid changes in the polarity of applied ac-field. Pure $CoFe_2O_4$ nanoparticles got lower value of tanδ in $Co_{1-x}Ba_xFe_2O_4$; x = 0.25, 0.50, 0.75 and 1.0 nanoparticles as shown in the inset of Figure 8 and Table 1. The variation in the concentrations of substituent Barium in $Co_{1-x}Ba_xFe_2O_4$ nanoparticles enhanced the tanδ due to enhancement in the grain boundaries effects caused by increased surface to volume ratio. Ac-conductivity (σ_{ac}) of any dielectric material gives the information about facilitation of charges that can be obtained from formula, $\sigma_{ac} = \omega\varepsilon_r'\varepsilon_0 tan\delta$; where '$\varepsilon$' is the permittivity of free space and 'ω'is the angular frequency[29]. The σ_{ac} is the migration of charge carriers from grain boundaries instead of accumulation and producing polarization. The variation in σ_{ac} of $Co_{1-x}Ba_xFe_2O_4$; x = 0, 0.25, 0.50, 0.75 and 1.0 nanoparticles with frequency is shown in Figure 6. The σ_{ac}revealed lower values in the low frequency region and gave rising values with increased frequency as displayed in Figure 6. The variation in the values of σ_{ac} can be justified with the conduction mechanism in ferrite nanoparticles owed to the hopping of charges. At lower frequency regime, the insulating grain boundaries become more active which results in decrease in σ_{ac}, while the conduction of charge carriers enhanced due to more active grains in higher frequency region. Inset of Figure 6 and Table 1 show that σ_{ac} in $Co_{1-x}Ba_xFe_2O_4$; x = 0.25, 0.50, 0.75 and 1.0 nanoparticles increased with increasing concentrations of barium. The increase in the values of σ_{ac} with increased contents of barium is due to the fact that barium have higher ionic radii than Co. So, the hopping charge carriers upsurge in $Co_{1-x}Ba_xFe_2O_4$ nanoparticles due to some loosely bound charges as compared to pure $CoFe_2O_4$ nanoparticles that resulted in the enhancement of σ_{ac} of the material.

CONCLUSIONS

Barium doped $CoFe_2O_4$ {i.e. $Co_{1-x}Ba_xFe_2O_4$; x = 0, 0.25, 0.50, 0.75 and 1.0} nanoparticles were synthesized using chemical solgel method. XRD analysis confirmed the cubic spinel structure of $CoFe_2O_4$ nanoparticles and orthorhombic spinel structure of $BaFe_2O_4$ nanoparticles. It was observed that with the substitution of barium in $CoFe_2O_4$ nanoparticles, the crystallite size of $Co_{1-x}Ba_xFe_2O_4$ nanoparticles was increased due to

the larger atomic radius of barium. SEM images revealed that most of the nanoparticles have polygon shaped or flakes like morphology. The suppression in vibrational modes of $Co_{1-x}Ba_xFe_2O_4$ nanoparticles was observed which attributed to the distortions and stresses in the crystal structure originated due to insertion of high ionic radii of Barium in these nanoparticles. The dielectric analysis showed that capacitance, $\varepsilon_r^{'}$, $\varepsilon_r^{''}$, and tanδ got maximal values in low frequency regime and decreased with increasing frequency due to interfacial polarization. The σ_{ac}showed lower values in low frequency region due to more active grain boundaries and increased with increase in frequency owing to more active conducting grains in high frequency regime. Overall, all the dielectric parameters of $Co_{1-x}Ba_xFe_2O_4$ nanoparticles were enhanced with increased doping contents of barium which can be associated with number of factors such as, decrease in particle size, lesser electronegativity and higher ionic radii. These measurements and analysis suggest that due to high values of dielectric constants especially ac-conductivity, these $Co_{1-x}Ba_xFe_2O_4$ nanoparticles can be the superlative candidate for energy storage devices.

Conflict of Interest

Authors declare that the paper is original and has not been submitted or is not being considered for publication elsewhere. I also declare that all authors have seen and approved the manuscript.

References

1) Jia, H.; Liu, W.; Zhang, Z.; Chen, F.; Li, Y.; Liu, J.; Nie, Y. Monodomain MgCuZn ferrite with equivalent permeability and permittivity for broad frequency band applications. *Ceramics International* **2017**, *43* (8), 5974–5978, DOI: 10.1016/j.ceramint.2017.01.129, available at https://dx.doi.org/10.1016/j.ceramint.2017.01.129.
2) Fei, L.; Hu, Y.; Li, X.; Song, R.; Sun, L.; Huang, H.; Gu, H.; Chan, H. L. W.; Wang, Y. Electrospun Bismuth Ferrite Nanofibers for Potential Applications in Ferroelectric Photovoltaic Devices. *ACS Applied Materials & Interfaces* **2015**, *7* (6), 3665–3670, DOI: 10.1021/acsami.5b00069, available at https://dx.doi.org/10.1021/acsami.5b00069.
3) Praveena, K.; Chen, H.-W.; Liu, H.-L.; Sadhana, K.; Murthy, S. R. Enhanced magnetic domain relaxation frequency and low power losses in Zn2+ substituted manganese ferrites potential for high frequency applications. *Journal of Magnetism and Magnetic Materials* **2016**, *420*, 129–142, DOI: 10.1016/j.jmmm.2016.07.011, available at https://dx.doi.org/10.1016/j.jmmm.2016.07.011.
4) Mounkachi, O.; Lamouri, R.; Abraime, B.; Ez-Zahraouy, H.; Kenz, A. E.; Hamedoun, M.; Benyoussef, A. Exploring the magnetic and structural properties of Nd-doped Cobalt nano-ferrite for permanent magnet applications. *Ceramics International* **2017**, *43* (16), 14401–14404, DOI: 10.1016/j.ceramint.2017.07.209, available at https://dx.doi.org/10.1016/j.ceramint.2017.07.209.
5) Yang, C.; Wu, J.; Hou, Y. Fe3O4 nanostructures: synthesis, growth mechanism, properties and applications. *Chemical Communications* **2011**, *47* (18), 5130–5130, DOI: 10.1039/c0cc05862a, available at https://dx.doi.org/10.1039/c0cc05862a.
6) Fu, Y.; Chen, H.; Sun, X.; Wang, X. Combination of cobalt ferrite and graphene: High-performance and recyclable visible-light photocatalysis. *Applied Catalysis B: Environmental* **2012**, *111-112*, 280–287, DOI: 10.1016/j.apcatb.2011.10.009, available at https://dx.doi.org/10.1016/j.apcatb.2011.10.009.
7) Amiri, S.; Shokrollahi, H. The role of cobalt ferrite magnetic nanoparticles in medical science. *Materials Science and Engineering: C* **2013**, *33* (1), 1–8, DOI: 10.1016/j.msec.2012.09.003, available at https://dx.doi.org/10.1016/j.msec.2012.09.003.
8) Karimi, Z.; Mohammadifar, Y.; Shokrollahi, H.; Asl, S. K.; Yousefi, G.; Karimi, L. Magnetic and structural properties of nano sized Dy-doped cobalt ferrite synthesized by co-precipitation. *Journal of Magnetism and Magnetic Materials* **2014**, *361*, 150–156, DOI: 10.1016/j.jmmm.2014.01.016, available at https://dx.doi.org/10.1016/j.jmmm.2014.01.016.
9) Nongjai, R.; Khan, S.; Asokan, K.; Ahmed, H.; Khan, I. Magnetic and electrical properties of In doped cobalt ferrite nanoparticles. *Journal of Applied Physics* **2012**, *112* (8), 084321–084321, DOI: 10.1063/1.4759436, available at https://dx.doi.org/10.1063/1.4759436.
10) Bharathi, K. K.; Markandeyulu, G.; Ramana, C. V. Structural, Magnetic, Electrical, and Magnetoelectric Properties of Sm- and Ho-Substituted Nickel Ferrites. *The Journal of Physical Chemistry C* **2011**, *115* (2), 554–560, DOI: 10.1021/jp1060864, available at https://dx.doi.org/10.1021/jp1060864.
11) Bharathi, K. K.; Noor-A-Alam, M.; Vemuri, R. S.; Ramana, C. V. Correlation between microstructure, electrical and optical properties of nanocrystalline NiFe1.925Dy0.075O4 thin films. *RSC Adv.* **2012**, *2* (3), 941–948, DOI: 10.1039/c1ra00161b, available at https://dx.doi.org/10.1039/c1ra00161b.
12) Bharathi, K. K.; Markandeyulu, G.; Ramana, C. V. Enhanced Dielectric Property of Ni Ferrite by Sm and Ho Substitution. *Electrochemical and Solid-State Letters* **2010**, *13* (11), G98–G98, DOI: 10.1149/1.3479553, available at https://dx.doi.org/10.1149/1.3479553.
13) Bharathi, K. K.; Tackett, R. J.; Botez, C. E.; Ramana, C. V. Correlation between Structural, magnetic and dielectric properties of manganese substituted cobalt ferrite". *Journal of Applied Physics* **2011**, *109*, 7–510, DOI: 10.1063/1.4827416, available at https://doi.org/10.1063/1.4827416.
14) Zhong, X. L.; Liao, M.; Wang, J. B.; Xie, S. H.; Zhou, Y. C. Structural, ferroelectric, ferromagnetic, and magnetoelectric properties of the lead-free Bi3.15Nd0.85Ti3O12/CoFe2O4 double-layered thin film. *Journal of Crystal Growth* **2008**, *310* (12), 2995–2998, DOI: 10.1016/j.jcrysgro.2008.02.031, available at https://dx.doi.org/10.1016/j.jcrysgro.2008.02.031.
15) Fiebig, M. Revival of the magnetoelectric effect. *Journal of Physics D: Applied Physics* **2005**, *38* (8), R123–R152, DOI: 10.1088/0022-3727/38/8/r01, available at https://dx.doi.org/10.1088/0022-3727/38/8/r01.
16) Lo, C. C. H. Compositional Dependence of the Magnetomechanical Effect in Substituted Cobalt Ferrite for Magnetoelastic Stress Sensors. *IEEE Transactions on Magnetics* **2007**, *43* (6), 2367–2369, DOI: 10.1109/TMAG.2007.892536.
17) Paulsen, J. A.; Ring, A. P.; Lo, C. C. H.; Snyder, J. E.; Jiles, D. C. Manganese-substituted cobalt ferrite magnetostrictive materials for magnetic stress sensor applications. *Journal of Applied Physics* **2005**, *97* (4), 044502–044502, DOI: 10.1063/1.1839633, available at https://dx.doi.org/10.1063/1.1839633.
18) Gunjakar, J. L.; More, A. M.; Shinde, V. R.; Lokhande, C. D. Synthesis of nanocrystalline nickel ferrite (NiFe2O4) thin films using low temperature modified chemical method. *Journal of Alloys and Compounds* **2008**, *465* (1-2), 468–473, DOI: 10.1016/j.jallcom.2007.10.130, available at https://dx.doi.org/10.1016/j.jallcom.2007.10.130.
19) Lee, G.; Park, J. Y.; Kim, C. S. Growth of ultra-fine cobalt ferrite particles by a sol-gel and their magnetic properties. *Journal*

of Materials Science **1998**, *33*, 3965–3968, DOI: 10.1023/A:1004696729673, available at https://doi.org/10.1023/A:1004696729673.

20) Okauno, N.; Hanshimoto, S.; Inomata, K. Preferred crystal orientation of cobalt ferrite thin films induced by ion bombardment during deposition". *Journal of Applied Physics* **1992**, *71*, 5926–5926, DOI: 10.1063/1.350442, available at https://doi.org/10.1063/1.350442.
21) Akhtar, K.; Gul, M.; Haq, I. U.; Khan, R. A.; Khan, Z. U.; Hussain, A. Synthesis and characterization of uniform fine particles of pure and chromium-substituted manganese ferrite with low dielectric losses. *Ceramics International* **2016**, *42* (16), 18064–18073, DOI: 10.1016/j.ceramint.2016.08.096, available at https://dx.doi.org/10.1016/j.ceramint.2016.08.096.
22) Kumar, E. R.; Kamzin, A. S.; Prakash, T. Effect of particle size on structural, magnetic and dielectric properties of manganese substituted nickel ferrite nanoparticles. *Journal of Magnetism and Magnetic Materials* **2015**, *378*, 389–396, DOI: 10.1016/j.jmmm.2014.11.019, available at https://dx.doi.org/10.1016/j.jmmm.2014.11.019.
23) Yousuf, M. A.; Baig, M. M.; Waseem, M.; Haider, S.; Shakir, I.; Khan, S. U.-D.; Warsi, M. F. Low cost micro-emulsion route synthesis of Cr-substituted MnFe2O4 nanoparticles. *Ceramics International* **2019**, *45* (17), 22316–22323, DOI: 10.1016/j.ceramint.2019.07.259, available at https://dx.doi.org/10.1016/j.ceramint.2019.07.259.
24) Rahman, M. T.; Vargas, M.; Ramana, C. V. Structural characteristics, electrical conduction and dielectric properties of gadolinium substituted cobalt ferrite. *Journal of Alloys and Compounds* **2014**, *617*, 547–562, DOI: 10.1016/j.jallcom.2014.07.182, available at https://dx.doi.org/10.1016/j.jallcom.2014.07.182.
25) Samad, R.; ud Din Rather, M.; Asokan, K.; Want, B. Magneto-dielectric studies on multiferroic composites of Pr doped CoFe2O4 and Yb doped PbZrTiO3. *Journal of Alloys and Compounds* **2018**, *744*, 453–462, DOI: 10.1016/j.jallcom.2018.01.403, available at https://dx.doi.org/10.1016/j.jallcom.2018.01.403.
26) Mandal, S. K.; Singh, S.; Dey, P.; Roy, J. N.; Mandal, P. R.; Nath, T. K. Temperature and frequency dependence of AC electrical properties of Zn and Ni doped CoFe2O4 nanocrystals. *Philosophical Magazine* **2017**, *97* (19), 1628–1645, DOI: 10.1080/14786435.2017.1312021, available at https://dx.doi.org/10.1080/14786435.2017.1312021.
27) Chakrabarty, S.; Pal, M.; Dutta, A. Yttrium doped cobalt ferrite nanoparticles: Study of dielectric relaxation and charge carrier dynamics. *Ceramics International* **2018**, *44* (12), 14652–14659, DOI: 10.1016/j.ceramint.2018.05.091, available at https://dx.doi.org/10.1016/j.ceramint.2018.05.091.
28) Rezlescu, N.; Rezlescu, E.; Pasnicu, C.; Craus, M. L. Effects of the rare-earth ions on some properties of a nickel-zinc ferrite. *Journal of Physics: Condensed Matter* **1994**, *6* (29), 5707–5716, DOI: 10.1088/0953-8984/6/29/013, available at https://dx.doi.org/10.1088/0953-8984/6/29/013.
29) Mubasher,; Mumtaz, M.; Hassan, M.; Ali, L.; Ahmad, Z.; Imtiaz, M. A.; Aamir, M. F.; Rehman, A.; Nadeem, K. Comparative study of frequency-dependent dielectric properties of ferrites MFe2O4 (M=Co, Mg, Cr and Mn) nanoparticles. *Applied Physics A* **2020**, *126* (5), 334–334, DOI: 10.1007/s00339-020-03529-y, available at https://dx.doi.org/10.1007/s00339-020-03529-y.
30) Mubasher,; Mumtaz, M.; Nazir, H.; Hussain, B.; Ullah, S.; Ali, M. AC-conduction mechanism in SiO2-coated BaFe2O4 nanoparticles. *Applied Physics A* **2022**, *128* (4), 285–285, DOI: 10.1007/s00339-022-05421-3, available at https://dx.doi.org/10.1007/s00339-022-05421-3.
31) Atif, M.; Nadeem, M.; Khalid, W.; Ali, Z. Structural, magnetic and impedance spectroscopy analysis of (0.7)CoFe2O4+(0.3)BaTiO3 magnetoelectric composite. *Materials Research Bulletin* **2018**, *107*, 171–179, DOI: 10.1016/j.materresbull.2018.07.026, available at https://dx.doi.org/10.1016/j.materresbull.2018.07.026.